12-26-2008

Final report: Task 22 — Extreme ground motion studies

John G. Anderson
University of Nevada, Reno, jga@seismo.unr.edu

James N. Brune
University of Nevada, Reno, brune@seismo.unr.edu

Jaak J.K. Daemen
University of Nevada, Reno, daemen@mines.unr.edu

Matthew Purvance
University of Nevada, Reno

Nevada System of Higher Education

TECHNICAL REPORT

FINAL REPORT: TASK 22-EXTREME GROUND MOTION STUDIES

Report Document Identifier:
TR-NQ-022-1

Cooperative Agreement # DE-FC28-04RW12232
Project Activity ORD-FY06-022

26 December 2008

REVISION: 0

Authors: John Anderson, James Brune, Jaak Daemen, Matthew Purvance

Principal Investigators: James N. Brune and John G. Anderson

FINAL REPORT: TASK 22-EXTREME GROUND MOTION STUDIES (SIP-UNR-049)

Preamble

TASK 22 consisted of two separate investigations into extreme ground motions due to seismic events, Subtask 1 and Subtask 2. Subtask 1 included field studies of geological formations that should put an upper bound on extreme ground motions that have happened at the site of the formations. The locations are critically selected to provide the most effective constraints possible on the validity of the probabilistic seismic hazard analysis for Yucca Mountain. Subtask 2 surveyed recorded ground motions from around the world, with the aim to draw general conclusions from these as to the conditions where extreme ground motions are observed. Recommendations for research concerning extreme ground motions were presented by Hanks et al. (2004 a,b). Preliminary results and feasibility conclusions were presented in a synthesis report by Brune et al. (2007, Synthesis Report).

SUBTASK 1: CONSTRAINTS ON YUCCA MOUNTAIN EXTREME GROUND MOTIONS BASED ON PRECARIOUSLY BALANCED ROCKS AND UNSTABLE PRECIPITOUS CLIFFS AT YUCCA MOUNTAIN, AND UN-FRACTURED SANDSTONES ALONG THE SAN ANDREAS FAULT.

INTRODUCTION

Probabilistic seismic hazard analysis (PSHA) is based on statistical assumptions which are questionable when extended to very low probability ground motions with annual occurrence probabilities of less than perhaps 10^{-6}. The assumption of ground motion lognormality results in ground accelerations of the order of 10 g along with 10 m/s ground velocities when extrapolated to such low probability events. The short historical database of instrumental recordings is not sufficient to determine the validity and inherent uncertainties of the statistical assumptions regarding the ground motion distributions. This lack of fundamental ground motion data suggests that we look for alternate methods to constrain ground motions over long time periods. In this vein we have investigated relic geomorphic and geologic ground motion indicators. As the PSHA derived ground motion amplitudes are so large, we might expect to find evidence of their occurrences should they have occurred in recent geologic time. Such evidence considered here includes: lack of precariously balanced rocks (perhaps 10 ka to 80 ka age constraint), rock avalanches from (formerly) unstable cliffs (perhaps a few hundred ka age constraint), and fractures in 5 ma sandstones along the San Andreas fault in California. The latter, due to the significantly higher rate of seismicity near the San Andreas fault, provides about 200 times as long of an equivalent time sample as is available at Yucca Mountain. Interpretation based on preliminary non-QA'd age dating suggests that we would be able to provide ground motion constraints for the last several hundreds of thousands of years to perhaps millions of years, and that these constraints would be considerably lower than estimates based on the extant Yucca Mountain PSHA.

PRECARIOUS ROCK CONSTRAINTS ON EXTREME GROUND MOTIONS

As a result of the discovery of numerous precariously balanced rocks in the vicinity of Yucca Mountain, a methodology has been developed to use these rocks to constrain the probable ground motions at the proposed repository location (Anooshepoor et al., 2004,2006). The precarious rock methodology gives a direct indication of the upper bound on the amplitude of past ground shaking at the precarious rock site. In other words precariously balanced rocks provide estimates of the ground motion amplitudes which have not been exceeded during the residence times of the precarious rocks. This information is in direct contrast to indirect inferences on ground motion amplitudes obtained from trenching studies at Yucca Mountain which cannot directly constrain ground motion amplitudes associated with observed fault slip evidence.

We previously presented estimates of unexceeded peak ground acceleration obtained from observations of precarious or toppled rocks at the Nevada Test Site (NTS) (Brune et al., 2003). Subsequently we improved our estimates by field-testing precarious rocks and by undertaking shake table tests utilizing recorded earthquake and nuclear explosion ground motions(Anooshepoor et al., 2004, 2006).

COSMOGENIC AGE DATING OF PRECARIOUS ROCK PEDESTALS

Prior to the research reported here we collected samples from precarious rock pedestals in Solatario Canyon for non-QA'd whole rock ^{36}Cl analyses (Brune et al., 2007, Synthesis Report). In addition rock varnish samples were collected and analyzed via the varnish microlamination method (VML) to determine the minimum surface exposure ages (Bell et al. 1998; Brune et al., 2007, Synthesis Report). The zero erosion cosmogenic age dates for precarious rock pedestals all exceed the minimum exposure ages based on varnish microlaminations. This is not unexpected as the varnish dates are minimum dates because the rock varnish formation process can be "reset' by periods of intense weathering, as might be expected during ice ages or during intense range-front fires. ^{36}Cl derived cosmogenic pedestal ages range from about 56 ka to 240 ka, with most values falling within 50-80 ka. These are considerably older than the minimum dates from rock varnish (generally ~12.5 ka). Thus these preliminary analyses suggested that these dates are consistent with the conclusions of Brune and Whitney (2002) that no large ground motions (greater than about 0.3 g have occurred since the most recent large event proposed from trenching studies (about 70 ka ago on the Solitario Canyon fault, and about 90 ka ago on the Paintbrush Canyon fault). The results further supported the conclusion that the erosion rates at Yucca Mountain are very low and that portions of the slopes at Yucca Mountain are extremely stable, with surface age dates of tens of thousands of years on exposed rocks The cosmogenic age dating results obtained during this project were carried out by John Whitney and Co-workers, and are described in a separate report (Whitney et al., 2008).

CONCLUSION FOR PRECARIOUS ROCKS

The relatively large horizontal ground accelerations predicted for 10^4 or more years by the recently completed Yucca Mountain PSHA (Stepp et al., 2001) are apparently not consistent with the preliminary results from precarious rock surveys, nor the results found by the research presented here and in the Synthesis Report (Appendix 4). Therefore we anticipate that further testing of precarious rocks and further QA'd cosmogenic age dating will provide improved constraints on the questionable statistical assumptions which lead to extremely high ground motion predictions at very low probabilities.

UNSTABLE PRECIPITOUS CLIFFS IN THE VICINITY OF YUCCA MOUNTAIN

In addition to numerous precarious and semi-precarious rocks in the vicinity of Yucca Mountain, our surveys have identified a plethora of unstable cliff faces on the western flanks of Yucca Mountain (Figure X). These formations consist of noncohesive, jointed rock units which are fragile when shaken by strong ground motions. Such cliffs are common throughout the area and result from differential erosion of welded and un-welded tuffs. These cliffs appear to be obviously unstable with regard to horizontal ground shaking. In addition these features appear to be persistent features of the Yucca Mountain landscape; as Yucca Mountain has been uplifted over time by the Solitario Canyon fault, erosion has occurred on the western flanks of the mountain leading to the continual exhumation of such jointed cliff units. Brune et al. (2005) suggested that these cliffs give a constraint on ground motions of a few tenths g over periods of the order of 100 ka. Preliminary results of modeling the dynamic response of these cliffs to extreme ground motions were reported in the Synthesis Report (Brune et al., 2007). Additionally Purvance et al. (2007) determined fragilities for 2-d cliff models with various joint orientations. The jointing patterns include subhorizontal, inclined, and random Voronoi joint sets as shown in Figure X. The waveforms chosen for this analysis were a subset of the maximum ground motion recordings catalogued by John Anderson and detailed later in this report. Specifically 20 waveform sets (e.g., horizontal and vertical recordings) were chosen with a broad range of PGV/PGA values. These particular waveforms were chosen based on our previous experience determining the overturning fragilities of freestanding blocks. The horizontal acceleration time histories were scaled from 0.2 g to 2.4 g and the horizontal to vertical PGA ratios were maintained. Cliff failure was defined in this work as the downhill migration of cliff face elements. These simulations were undertaken using the Universal Distinct Element Code (UDEC) developed by Itasca Consulting. Figure X shows these preliminary cliff fragilities. These fragilities are rough due to the very limited number of waveforms used in their determination. Notice that the jointing orientations significantly affect the cliff fragilities. In particular the presence of inclined joint sets may allow for cliff units to withstand significantly higher accelerations than subhorizontal joint sets. Field investigations have indicated that a number of cliff features contain slightly (~10-15 degree) inclined joints sets. Further analyses are required to assess the fragilities of cliff units with realistic joint inclinations. Purvance et al.

(2007) also calculated the cliff responses when exposed to the Yucca Mountain 10^{-5} and 10^{-6} design ground motions outlined in Wong and Stepp (1998). Those ground motions were developed based on the fore mentioned PSHA results of Stepp et al. (2001). Over one half of the 16 10^{-5} ground motions and nearly all of the 10^{-6} ground motions would destroy cliff units with subhorizontal jointing patterns. Thus it is clear that extreme ground motions would destroy such cliffs.

NTS MEGA-BRECCIA ROCK AVALANCHES: CORRELATION WITH GROUND MOTION PREDICTIONS FROM LARGE UNDERGROUND NUCLEAR EXPLOSIONS.

North of Yucca Mountain on NTS, cliff faces on Pahute Mesa have been shaken down by ground motions resulting from energetic underground nuclear explosions (UNEs). Very near to large UNEs, precariously balanced rocks are conspicuously absent from the landscape. In addition, cliff faces are shattered and exhibit numerous, recent rockfalls resulting in mega-breccia rock avalanches. These are evidenced by fresh white surfaces covered by caliche (calcium carbonate) and chalcedony (silica), providing a clear indication that the rockfalls have been caused by the UNEs. Subsequently John Whitney and coworkers have extradited aerial photographs from the USGS archives of some cliff units on Pahute Mesa before and after powerful UNEs, confirming that indeed the mega-breccias are geomorphic indicators of the UNE induced extreme ground motions. As distance from the UNEs increases, rock avalanches disappear and fewer rockfalls are observed (Brune et al. (199x?).

In May 2005 we carried out a reconnaissance field survey of sites of rock avalanches created by large UNE shots. We estimated the peak ground accelerations and velocities from empirically derived ground motion prediction equations for UNEs. From these standard ground motion prediction equations of yield and distance, it was concluded that some of the sites of rock avalanches were exposed to ground accelerations of several g and ground velocities of a few m/s. Ground motions of this amplitude are in the range of those produced by Yucca Mountain PSHA and are truly extreme ground motions. Very large blocks of rock, up to several meters in dimension, were moved 10s of meters horizontally and thrown downhill to form very impressive mega-breccias. The fact that such large blocks of rock could undergo such large displacements testifies to the huge energies involved. Inspection of the size distribution of members of these UNE induced mega-breccias has revealed that the in situ joint distribution strongly affects the boulder size distribution. Conchoidal fractures are also observed in areas without developed joints. The presence of pervasive cooling joints in the Topopah and Teva Canyon Tuffs of Yucca Mountain suggests that should such extreme ground motions have occurred at Yucca Mountain, one might expect similar mega-breccias to be present in Solitario Canyon. This contrasts sharply with the precipitous cliffs existing at Yucca Mountain and the absence of large rubble piles below the cliff faces. In fact there is no evidence that rock avalanches of this type have ever existed at Yucca Mountain. The time constraint associated with the lack of evidence for rock avalanches at Yucca Mountain is the time for natural processes to eliminate the evidence of such rock avalanches which is probably of the order of 10^5 years or longer. There are a few large boulders on the pediment (little or no alluvium) at the north end of Solitario Canyon. Cosmogenic age dates on some of these boulders, as well as boulders in other environments, including cliffs and colluvium at Yucca Mountain, provide estimates of erosion rates of boulders

exposed to subaerial processes. Results of cosmogenic and geomorphic studies are reported in the associated study of Whitney et al. (2008).

CONCLUSION FROM UNSTABLE PRECIPITOUS CLIFFS AT YUCCA MOUNTAIN

A useful constraint on strong ground motions at Yucca Mountain can be obtained by estimating the time it would take for shaken down cliffs, with consequent rock avalanches (piles of rubble at the cliff base forming mega-breccias) to be re-eroded to unstable conditions similar to those observed currently (no mega-breccias at the base of the cliffs and many unstable cliff units). Preliminary estimates based on cosmogenic age dating described above, suggest that hundreds of ka or greater would be required for such evidence of extreme ground motions to be removed from the landscape. These results suggest that such large ground motions have not occurred at Yucca Mountain for at least this time period.

CONSTRAINTS ON EXTREME GROUND MOTIONS FROM UNFRACTURED SANDSTONES ALONG THE SAN ANDREAS FAULT

Large sandstone outcrops occur at several locations within 5 km of the San Andreas fault between Tejon Pass and Cajon Pass. These sandstones are greater than 5 million years old**.** Motion on the San Andreas Fault in this region commenced about **5** million years ago. Thus these rocks have been exposed to San Andreas fault earthquakes for about 5 million years. At the current inferred rate of occurrence of large earthquakes, this might translate into as many as 20,000 M ~ 8 events occurring within ~ 5 km of these sandstone outcrops, with about 200 occurring in the last 50 ka. The equivalent comparable time scale translated to Yucca Mountain would be more than a billion years as the rate of seismicity is about 200 times lower at Yucca Mountain. Preliminary measurements of tensile strength of surface samples of the San Andreas sandstones indicate values of less than 15 bars. Should these values correspond to the true tensile strength of the bulk sandstone at depth, the lack of clear evidence of sandstone failure provides constraints on the maximum levels of ground motion that have not been exceeded during their residence times. If particle velocities exceeded about 1 m/s at about ¼ wavelength depth, the internal strains caused by the dynamic stresses would fracture the sandstones in tension. There is no evidence of such tensional fracturing features in these sandstones as has been documented by Brune (2006).

In order to quantify these estimates, the following activities were carried out for Subtask 1:

1. We measured the shear-wave velocities of the sandstones. Fracture or lack of fracture depends on the shear strains in the rock, which in turn are proportional to particle velocity divided by shear-wave velocity. The shear wave velocities observed ranged from xx m/s at shallow depth to about 2 km/s at 1000 m depth. The details of the results of this study are reported in detail in Appendix 1.
2. We measured the tensile strength of a number of samples of the sandstones. Many measurements indicated tensile strengths of the order of 5 bars or less. Due to the weak

nature of the samples and uncertainties in the interpretation of tensile strength results when compared to results from compression tests, we conservatively estimate that the tensile strengths are less than 15 bars. The detailed results of these measurements are reported in Appendix 2.

3. We calculated tensile and shear stresses as a function of depth resulting from combinations of lithostatic stresses and transient dynamic stresses from thousands of large (M~8) earthquakes. If the tectonic stresses are large enough, relatively low amplitude transient stresses would have fractured the rock at depths less than about 1 km in tension or in shear. A detailed description of these calculations is described in Appendix 3.

CONCLUSIONS FROM UNFRACTURED SANDSTONES ALONG THE SAN ANDREAS FAULT

Un-fractured Tertiary sandstones exist within ~ 5 km of the San Andreas fault at several locations between Cajon Pass and Tejon Pass. These sandstones have been exposed to three stresses: lithostatic stresses from overburden when buried, tectonic stresses related to the faulting, and transient dynamic stresses from thousands of large M ~ 8 earthquakes. If the tectonic stresses are large enough, relatively low amplitude transient dynamic stresses will fracture the rock at depths less than about 1 km. Thus the observation that the sandstones are un-fractured places an upper bound on the combination of tectonic stresses and extreme transient dynamic stresses.

Preliminary measurements of tensile strengths of un-fractured sandstones at several sites near the fault yield values less than 15 bars with 95% confidence. In addition, many of the tensile strength measurements produce values less than 10 bars. The rocks at these sites have been at depths between 1 km and 0 km (the surface) during the history of the San Andreas fault. ReMI measurements of shear wave velocity provide input for calculations of strain as a function of particle velocity. Thus the un-fractured sandstones are evidence against the extreme ground motions (> 2 m/s, very low probability) being considered in the design of the designated nuclear waste repository at Yucca Mountain, Nevada.

Subtask 2: Prepare summary report on large recorded ground motions

The final report for Subtask 2, TR-NQ-02202 (Anderson, 2008), was approved and submitted in January 2008.

This subtask aimed to understand the characteristics of the free-field strong-motion records that have yielded the 100 largest peak accelerations and the 100 largest peak velocities recorded to date. The peak is defined as the maximum magnitude of the acceleration or velocity vector during the strong shaking. This compilation includes 35 records with peak acceleration greater than gravity, and 41 records with peak velocities greater than 100 cm/s. The results represent an estimated 150,000 instrument-years of strong-motion recordings. The mean horizontal acceleration or velocity, as used for the NGA ground motion models, is typically 0.76 times the magnitude of this vector peak. Accelerations in the top 100 come from earthquakes as small as magnitude 5, while velocities in the top 100 all come from earthquakes with magnitude 6 or larger. Records are dominated by crustal earthquakes with thrust, oblique-thrust, or strike-slip mechanisms. Normal faulting mechanisms in crustal earthquakes constitute under 5% of the records in the databases searched, and an even smaller percentage of the exceptional records. All NEHRP site categories have contributed exceptional records, in proportions similar to the extent that they are represented in the larger database.

References

Allen, B.M., Drellack, S.L., Jr., Townsend, M.J. (1997). Surface Effects of Underground Nuclear Explosions: U.S. Department of Energy Report DOE/NV/11718-122.

Anderson, J.G. (2008). Source and site characteristics of earthquakes that have cause exceptional ground accelerations and velocities, *Bull. Seismol. Soc. Amer*. **98** (submitted).

Anderson, J. G. (2008). Exceptional Ground Accelerations and Velocities Caused by Earthquakes, Final Technical Report TR-NQ-022-2, Task ORD-FY06-022, Subtask 2, Nevada System of Higher Education.

Andrews, D. J., T. C. Hanks, and J. W. Whitney (2007). Physical limits on ground motion at Yucca Mountain, *Bull. Seismol. Soc. Amer*. **97**, 1771-1792.

Anooshehpoor, A. and Brune, J. N. (1997). Precarious rock methodology: field and laboratory test results, Data Package, Activity Number 8.3.1.17.4.1.2, Accession Number MOL.19970626.0464.

Anooshehpoor, A., J. N. Brune, and D. H. Von Seggern (2002), Constraints on ground motion at Yucca Mountain provided by precarious rocks, DOE/NSHE Cooperative Agreement Number DE-FC08-98NV12081, Report TR-02-001.

Anooshehpoor, A., Brune, J. N. and Zeng, Y. (2004). Methodology for obtaining constraints on ground motion from precariously balanced rocks, *Bull. Seism. Soc. Am.*, **94**, 285-303.

Anooshehpoor, R., Purvance, M. D., Brune, J. N., Preston, L. A., Anderson, J. G., and Smith, K. D. (2006). Precarious rock methodology for seismic hazard: physical testing, numerical modeling and coherence studies, DOE/NSHE Cooperative Agreement Task ORD-FY04-020, Final Technical Report TR-06-003.

BSC (2005). Peak Ground Velocities for Seismic Events at Yucca Mountain, Nevada, *Bechtel SAIC Company*, ANL-MGR-GS-000004 REV 00.

Bell, J. W., Brune, J. N., Liu, T., Zerda, M., and Yount, J. C. (1998). Dating the precariously balanced rocks in seismically active parts of California and Nevada, *Geology*, **26**, 495-498.

Bierman, P. R., and Caffee, M. W. (2002). Cosmogenic exposure and erosion history of ancient Australian bedrock landforms, *Geol. Soc. Am. Bull.*, **114**, 787-803.

Board, M.P. (2006). Background information to support nonlinear wave propagation studies for analysis of extreme ground motion at the Yucca Mountain site, *Itasca Consulting group, Inc.*, Minneapolis, Minnesota. *ExGM Synthesis Report.*

Brune, J.N., D. von Seggern, and A. Anooshehpoor (2003). Distribution of precarious rocks at the Nevada Test Site: comparison with ground motion predictions from nuclear tests, *J. Geophys. Res., 108*(B6), 2306, doi:10.1029?2002.JB002000, 2003.

Brune, J.N., K.D. Smith, and Y. Zeng (2005). Precarious rock evidence for seismic shaking during and prior to the 1992 M_L 5.6 Little Skull Mountain, Nevada, earthquake, *Earthquake Spectra, 21*, 967-985.

Brune, J.N., J.W. Whitney, J.G. Anderson, R. Anooshehpoor, R.C. Finkel, and M. Purvance (2007). Report on constraints on unexceeded ground motions based on precariously balanced rocks and unstable precipitous cliffs at Yucca Mountain and unfractured sandstones along the San Andreas fault. *ExGM Synthesis Report.*

Brune, J. N. (1996). Precariously balanced rocks and ground motion maps for southern California, *Bull. Seism. Soc. Am.*, **86**, 43-54.

Brune, J. N., D. von Seggern, and A. Anooshehpoor (2003). Distribution of Precarious Rocks at the Nevada Test Site: Comparison with Ground-Motion Predictions from Nuclear Tests, *J. Geophys. Res*., **108**, 2306, doi:10.1029/2002JB002000.

Brune, J.N., K.D. Smith, and Y. Zeng (2005). Precarious rock evidence for seismic shaking during and prior to the 1992 Ml 5.6 Little Skull Mountain, Nevada, Earthquake. *Earthquake Spectra* **21**(4), 967-985

Brune, J. N., and Whitney, J. W. (2000). Precarious Rocks and seismic shaking at Yucca Mountain, Nevada, *USGS Digital Data Series*, **058,** Chapter M.

Brune, J.N., M.D. Purvance, J. Daemen, J.S. Chester, and T. Tullis (2006). Unfractured sandstones along the San Andreas Fault: constraints on extreme ground motion and absolute stress, *Proceedings of the 2006 Annul SCEC Meeting*: Palm Springs, Calif., September 10-13.

BSC (2004). Technical Basis Document No. 14: Low Probability Seismic Events, Revision 1, OCRWM DCN #43222, Bechtel SAIC Company, LLC, Las Vegas, 306 pages.

Gosse, J. Harrington, C.D., and Whitney, J. W. (1996). Applications of in situ cosmogenic nuclides in the geologic site characterization of Yucca Mountain, Nevada, *Material Research Society Symposium Proceedings*, **412**, 799-806.

Gonzalez, S.H., A.P. Morris, G.I. Ofoegbu, K.J. Smart, and J.A. Stamatakos (2006). Review of "Peak Ground Velocities for Seismic Events at Yucca Mountain," *Center for Nuclear Waste Regulatory Analyses*, San Antonio, Texas.

Gosse, J.C., C.D. Harrington, and J.W. Whitney (1996). Applications of in situ cosmogenic nuclides in the geologic site characterization of Yucca Mountain, Nevada, *Mat. Res. Soc. Symp. Proc. Vol. 412*, 799-806.

Grasso, D.N. (2001). GIS Surface Effects Archive of Underground Nuclear Detonations Conducted at Yucca Flat and Pahute Mesa, Nevada Test Site, Nevada: USGS Open-File Report 01-272.

Hanks, T.C., N.A. Abrahamson, M. Board, D.M. Boore, J.N. Brune, and C.A. Cornell (2004). Observed ground motions, extreme ground motions, and physical limits to ground motions, *International Workshop on Future Directions in Instrumentation for Strong Motion and Engineering Seismology,* May 17-21, 2004 Kusadasi, Turkey.

Hanks, T.C., Chair, Abrahamson, N.A., Board, M., Boore, D.M., Brune, J.N., and Cornell, C.A., Workshop Committee, 2006, Report of the Workshop on Extreme Ground Motions at Yucca Mountain, August 23-25, 2004: U.S. Geological Survey Open-File Report 2006-1277 [available on the World Wide Web at http://pubs.usgs.gov/of/2006/1277/].

Hanks, T.C., Abrahamson, N.A., Board, M., Boore, D.M., Brune, J.N., and Cornell, C.A., 2005, Observed ground motions, extreme ground motions, and physical limits to ground motions, in Future Directions of Strong Motion Instrumentation, P. Gulkan and J.G. Anderson, eds., Springer, The Netherlands.

Harris, R.A., M. Barall, R. Archuleta, B. Aagard, J.P. Ampuero, H. Bhat, L. Dalguer, S. Day, B. Duan, E, Dunham, G. Ely, Y. Kase, N. Lapusta, Y. Liu, S. Ma, D. Oglesby, K. Olsen, A. Pitarka, and E. Templeton (2007). The SCEC/USGS earthquake dynamics code validation exercise, *Workshop on Numerical Modeling of Earthquake Source Dynamics*, Bratislava, Slovak Republic.

Harris, R.A., M. Barall, R. Archuleta, E. Dunham B. Aagard, J.P. Ampuero, H. Bhat, V. Cruz-Atienza L. Dalguer, P. Dawson, S. Day, B. Duan, , G. Ely, Y. Kaneko, Y. Kase, N. Lapusta, Y. Liu, S. Ma, D. Oglesby, K. Olsen, A. Pitarka, S. Song and E. Templeton (2008). The SCEC/USGS dynamic earthquake-rupture code verification exercise, submitted to *Seismological Research Letters*

Hecker, S., T.E. Dawson, and D.P. Schartz (2007). Maximum fault displacements in extensional regimes : a geological perspective (abstract), *International Union of Geology and Geophysics*, Perugia, Italy.

Keefer, W.R., Whitney, J. W., and Buesch, D., 2007, Geology of the Yucca Mountain Site Area: GSA Memoir 199 on the geology and climatology of Yucca Mountain, Chapter 3, p. 53-103.

Ma, Shuo (2008). A physical model for widespread near-surface an fault zone damage induced by earthquakes, submitted to GRL (?)

Murphy, J. M., and J. A. Lahoud (1969). Analysis of seismic peak amplitudes from underground nuclear detonations, *Bull. Seism.. Soc. Am*., **59**, 2325 –2342.

Nichols, K.K., Bierman, P.R., Foniri, W.R., Gillespie, A.R., Caffee, M., and Finkel. R., 2006, Dates and rates of arid region geomorphic processes: *GSA Today*, **16**, 4-10.

Perret, W.R., R.C. Bass (1975). Free-field ground motion induced by underground explosions, Technical Report No. SAND74-0252.

Purvance, M. D. (2005). Overturning of slender blocks: numerical investigation and application to precariously balanced rocks in southern California, *Ph.D. Dissertation*, University of Nevada, Reno, Reno, Nevada (http://www.seismo.unr.edu/gradresearch.html).

Purvance, M.D., Anooshehpoor, R. and Brune, J. N. (2006). Precariously balanced rock methodology and shake table calibration, *Seism. Res. Letts*., **77**, p. 246.

Stepp, J. C., I. Wong, J. Whitney, R. Quittmeyer, N. Abrahamson, G. Toro, R. Youngs, K. Coppersmith, J. Savy, T. Sullivan, and Yucca Mountain PSHA project Members (2001). Probabilistic seismic hazard analyses for fault displacement and ground motions at Yucca Mountain, Nevada, *Earthquake Spectra*, **17**, 113-152.

Vortmann, L. J. (1980). Prediction of ground motion from underground nuclear weapons tests as it relates to siting of a nuclear waste storage facility at NTS and compatibility with the weapons test program, Report SAND80-1020/1, Sandia National Laboratories, Albuquerque, New Mexico.

.

Whitney, J. W. And Harrington, C.D., 1993, Relict colluvial boulder deposits as paleoclimatic indicators in the Yucca Mountain region, southern Nevada, *Geol. Soc. Am. Bull.*, **105**, 1008-1018.

YM PSHA: Civilian Radioactive Waste Management System Management and Operating Contractor (1998). Probabilistic seismic hazard analyses for fault displacement and vibratory ground motion at Yucca Mountain, Nevada, Wong, I. G. and J. C. Stepp, report coordinators, U. S. Department of Energy, Oakland, California.

Appendix 1: Refraction Microtremor (ReMi) Results for San Andreas Sandstones

Introduction

To address the possibility that tensile strength and other properties of rock near the San Andreas Fault might show anomalous increases with depth (e.g., as a result of surface weathering), we have carried out refraction microtremor (Louie, 2001) measurements of shear velocities at several sandstone outcrops. These surveys give results as volume averages over tens of meters. This QA work was recorded in Scientific Notebook NSHE-UNR-108 Vol. 1 and the measurements were carried out in accordance with IPR-024. Software User Request SUR-06-014 covered the SeisOpt REMI V2.0 software used in the Vs30 analyses.

Data Acquisition

Shallow shear-wave velocities averaged from the surface to 30 m depth (Vs30) were measured at five sites using the refraction microtremor survey method. The site locations (center points of the arrays) are as follows:

Lines 101 and 102: 34.31454N 117.46626W
Line 103: 34.31861N 117.50412W
Line 106: 34.41622N 117.85700W
Line 107: 34.63343N 118.32512W
Line 108: 34.76689N 118.78780W
Line 109: 34.76667N 118.78848

The sites are mapped in Figure 1, below. All site locations are close to the San Andreas Fault (shown as heavy red lines in Figure 1). Lines 101 and 102 have the same midpoint, but the recording instrument spacing for line 101 is 15 meters (the standard for these measurements); the spacing for line 102 is 8 meters. The locations of the recording seismographs as determined by individual GPS readings are shown in Figure 2. The purpose in deploying the nested arrays (lines) with different apertures is to determine whether the velocity-depth models derived after the data are processed are within the ±20% accuracy limits claimed for the method (Louie, 2001).

Data Processing

The data recordings were processed by the QA-approved Assemble Texans and SeisOpt REMI V2.0 software. All analyses were repeated by a second analyst and produced essentially identical results (see Sources of Error, below)

Sources of Error

The refraction microtremor method has a stated accuracy for Vs30 measurements of ±20% (Louie, 2001). The variation in Vs30 values obtained by different analysts working with

the same data sets (due to picking and modeling differences) was examined for a large-scale refraction microtremor survey and such variation was expected to be less than ±10% (Scott, et al., 2004). The analyses presented in Figures 3 through 9 were reviewed by another analyst and were deemed to be within this ±10% limit.

Summary and Conclusions

The shear wave velocities at the surface are between 400 m/s and 750 m/s, increasing to over 1000 m/s at 40 m to 100 m depth. Vs30 averaged for the five sites was 0.564 km/s. At greater depths, shear velocity increases to 1.0–2.0 km/s at 100 meters depth (the approximate depth limit for the refraction microtremor surveys). Corresponding P-wave velocities were not measured, but are estimated to be about 1.0 km/s when averaged from the surface to 30 m depth, and 1.7 - 3.5 km/s at 100 m depth. These results are typical at the surface for sedimentary outcrop of Tertiary or Quaternary age that is indurated, or is bouldery or cobbly. The changes in shear velocity within the upper 100 m of these monoliths is very similar to the velocity profiles of fluvial gravels (Thelen et al. 2006) and thus do not indicate drastically unusual rock properties.

The nested arrays of lines 101 and 102 yielded Vs30 values within ±0.3%, with minor variation in the velocity-depth models, in line with our expectations of variation due to the differences in the sizes of the array apertures.

References

Louie, J. N., 2001, Faster, better: shear-wave velocity to 100 meters depth from refraction microtremor arrays, Bull. Seis. Soc. Amer., **91,** 347-364.

Scott, J. B., M. Clark, T. Rennie, A. Pancha, and J. N. Louie, 2004. A shallow shear-wave transect across the Reno, Nevada, area basin, Bull. Seis. Soc. Amer., **94**, 2222-2228.

Thelen, W. A., M. Clark, C. T. Lopez, C. Loughner, H. Park, J. B. Scott, S. B. Smith, B. Greschke, and J. N. Louie, 2006, A transect of 200 shallow shear velocity profiles across the Los Angeles Basin: Bull. Seis. Soc. Amer., **96**, 1055-1067.

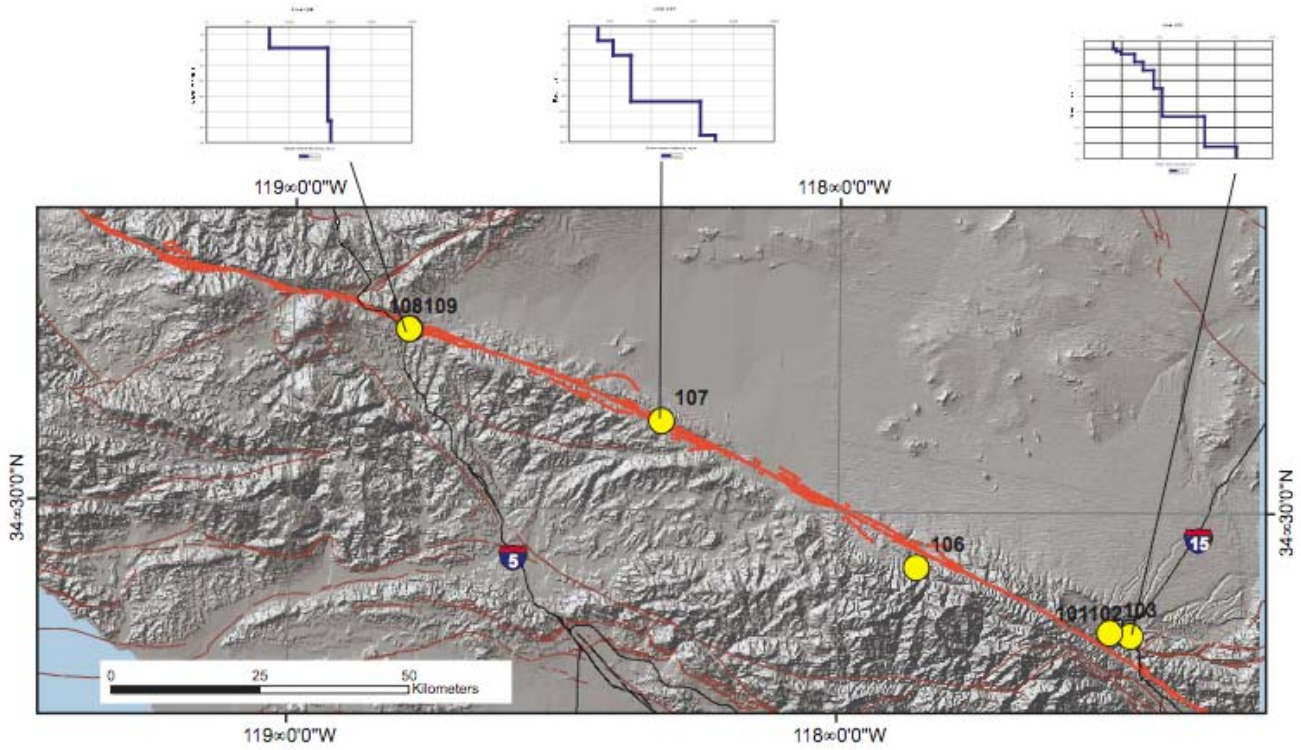

Figure 1. Map showing locations of the refraction microtremor surveys. The velocity-depth models for three of the arrays are shown above the map.

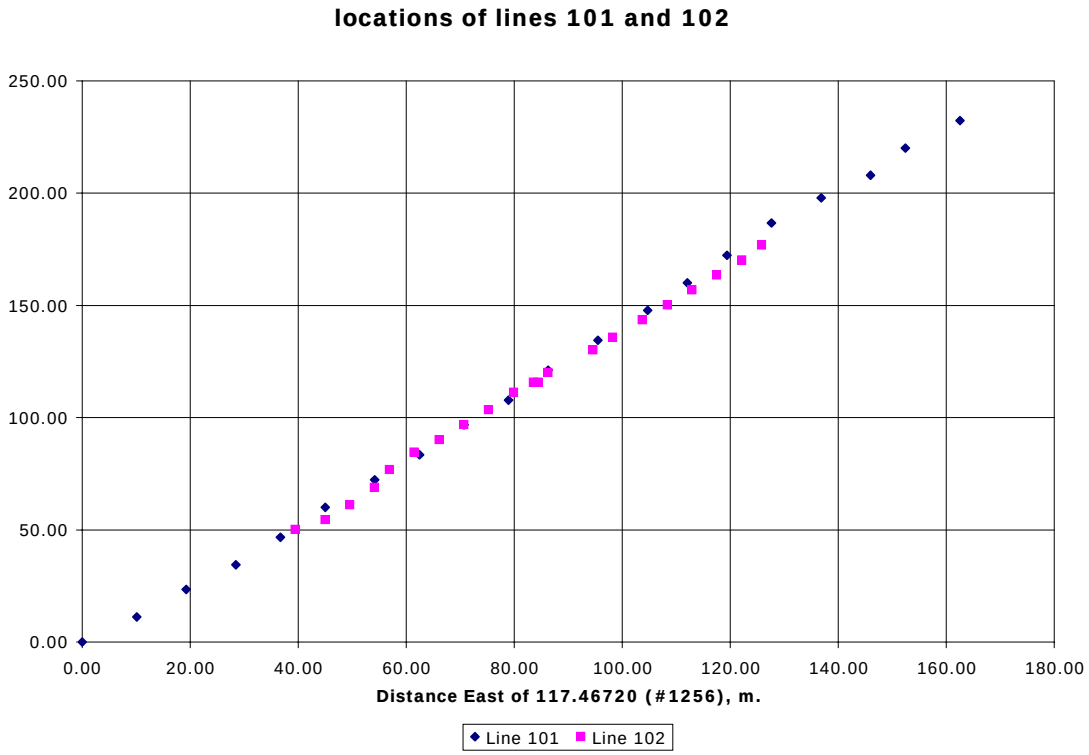

Figure 2. GPS locations of individual seismographs for lines 101 and 102.

Line 101 Analysis Results

Slowness vs. Frequency (p-f) Plot with Picks

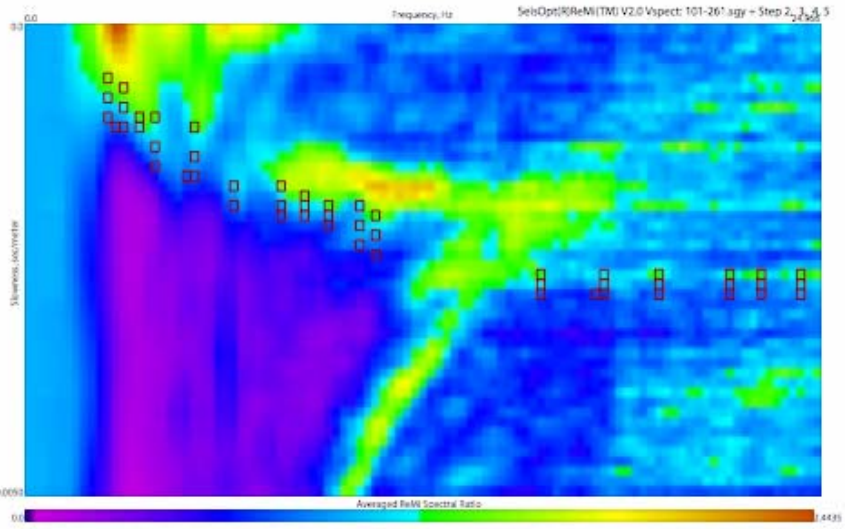

Vs vs. Depth Model

Vs, m/s	Depth, m
390.7	0.0
390.7	-10.5
428.3	-10.5
428.3	-13.3
494.1	-13.3
494.1	-16.6
672.6	-16.6
672.6	-26.6
785.3	-26.6
785.3	-37.5
926.3	-37.5
926.3	-60.3
1039.0	-60.3
1039.0	-96.4
1602.7	-96.4
1602.7	-134.9
2025.5	-134.9
2025.5	-234.9
Vs30=506	

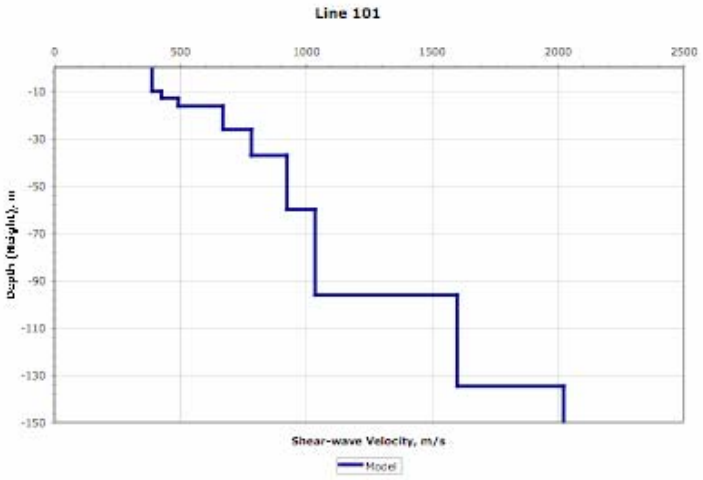

Figure 3. Analysis results for Line 101

Line 102 Analysis Results

Slowness vs. Frequency (p-f) Plot with Picks

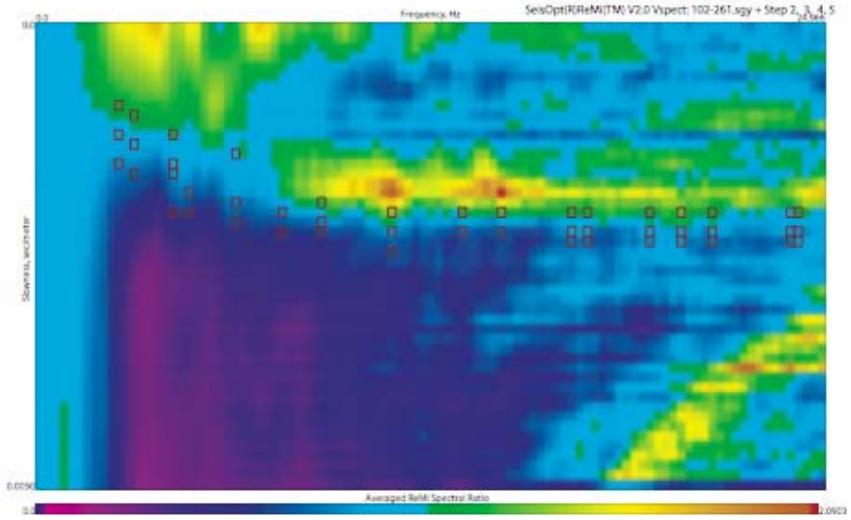

Vs vs. Depth Model

Vs, m/s	Depth, m
495.2	0.0
495.2	-26.6
575.1	-26.6
575.1	-45.6
883.3	-45.6
883.3	-88.6
1088.8	-88.6
1088.8	-133.0
1248.6	-133.0
1248.6	-233.0

Vs30=503

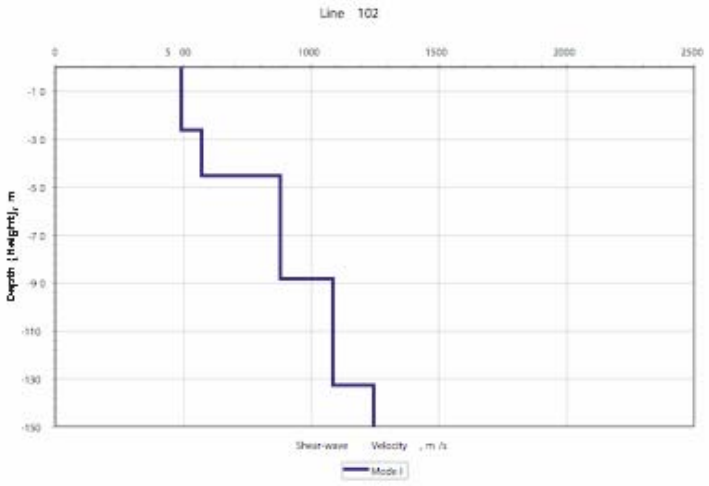

Figure 3. Analysis results for Line 102

Line 103 Analysis Results

Slowness vs. Frequency (p-f) Plot with Picks

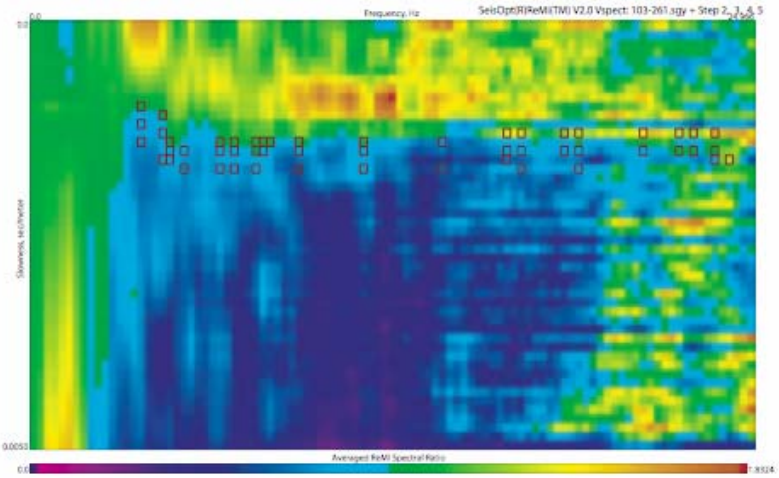

Vs vs. Depth Model

Vs, m/s	Depth, m
746.3	0.0
746.3	-98.3
2550.0	-98.3
2550.0	-106.9
2525.3	-106.9
2525.3	-206.9

Vs30=746

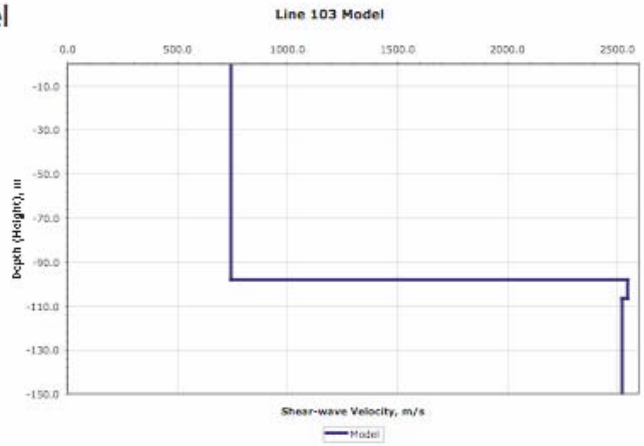

Figure 3. Analysis results for Line 103

Line 106 Analysis Results

Slowness vs. Frequency (p-f) Plot with Picks

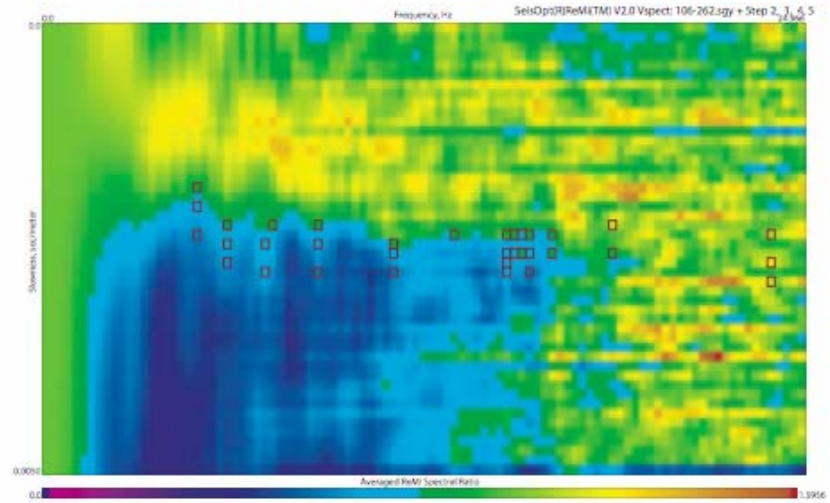

Vs vs. Depth Model

Vs, m/s	Depth, m
436.9	0.0
436.9	-40.4
1010.6	-40.4
1010.6	-92.2
1286.4	-92.2
1286.4	-192.2

Vs30=437 m/s

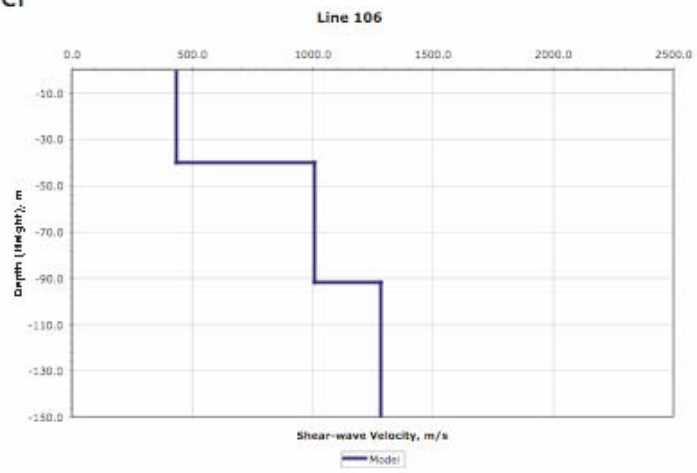

Figure 3. Analysis results for Line 106

Line 107 Analysis Results

Slowness vs. Frequency (p-f) Plot with Picks

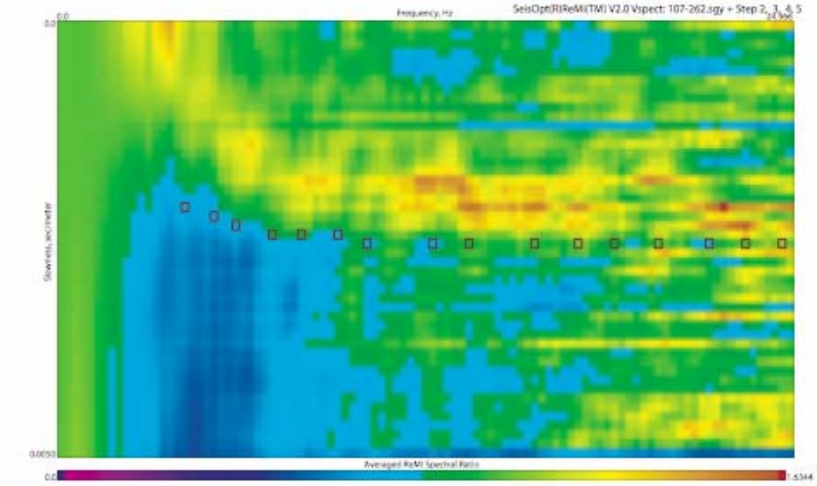

Vs vs. Depth Model

Vs, m/s	Depth, m
438.1	0.0
438.1	-27.1
529.5	-27.1
529.5	-41.1
582.5	-41.1
582.5	-96.0
1066.0	-96.0
1066.0	-196.0

Vs30=446

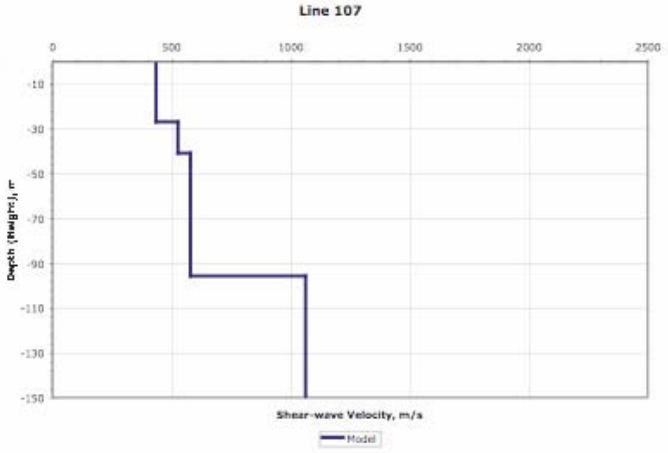

Figure 3. Analysis results for Line 107

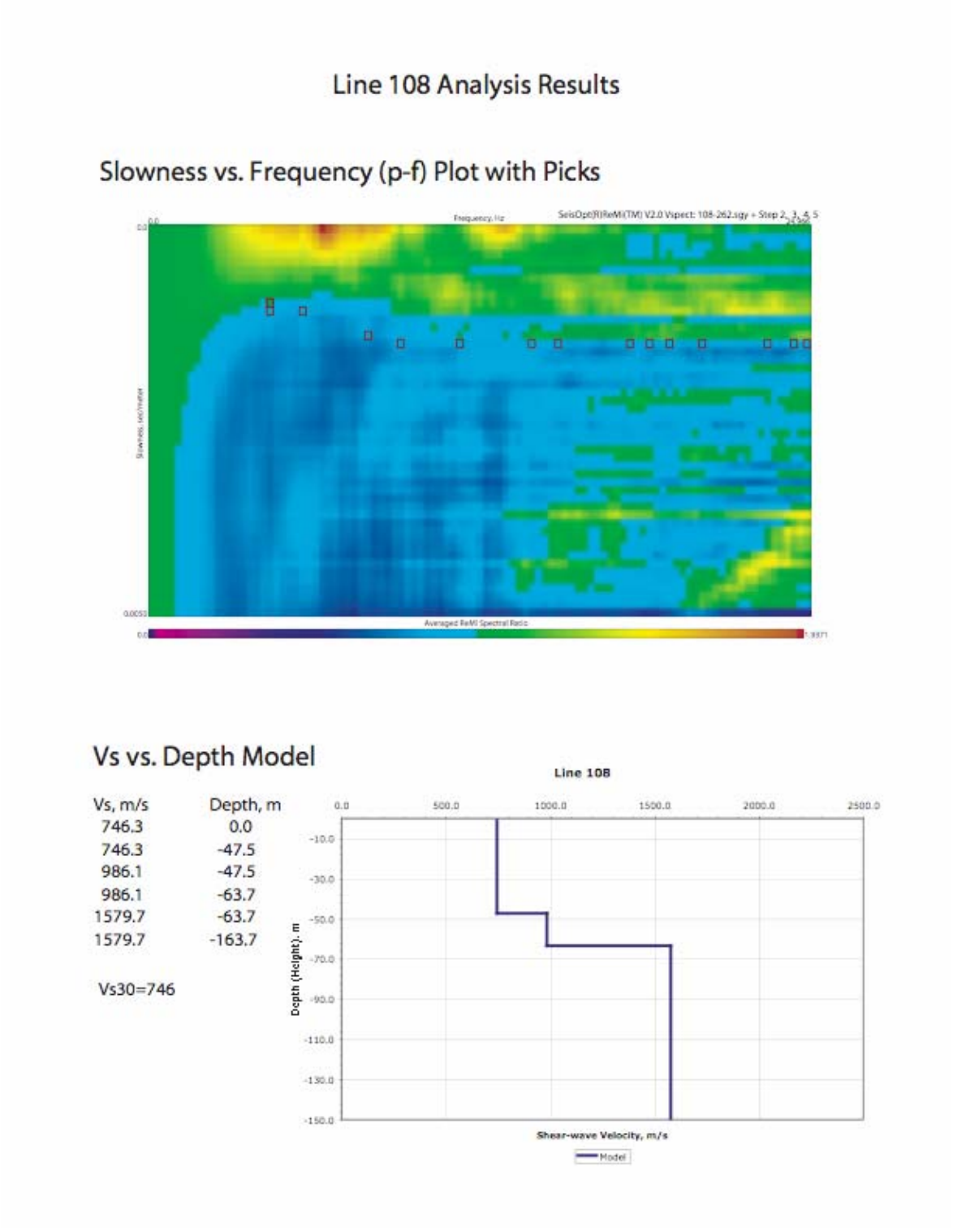

Figure 3. Analysis results for Line 108

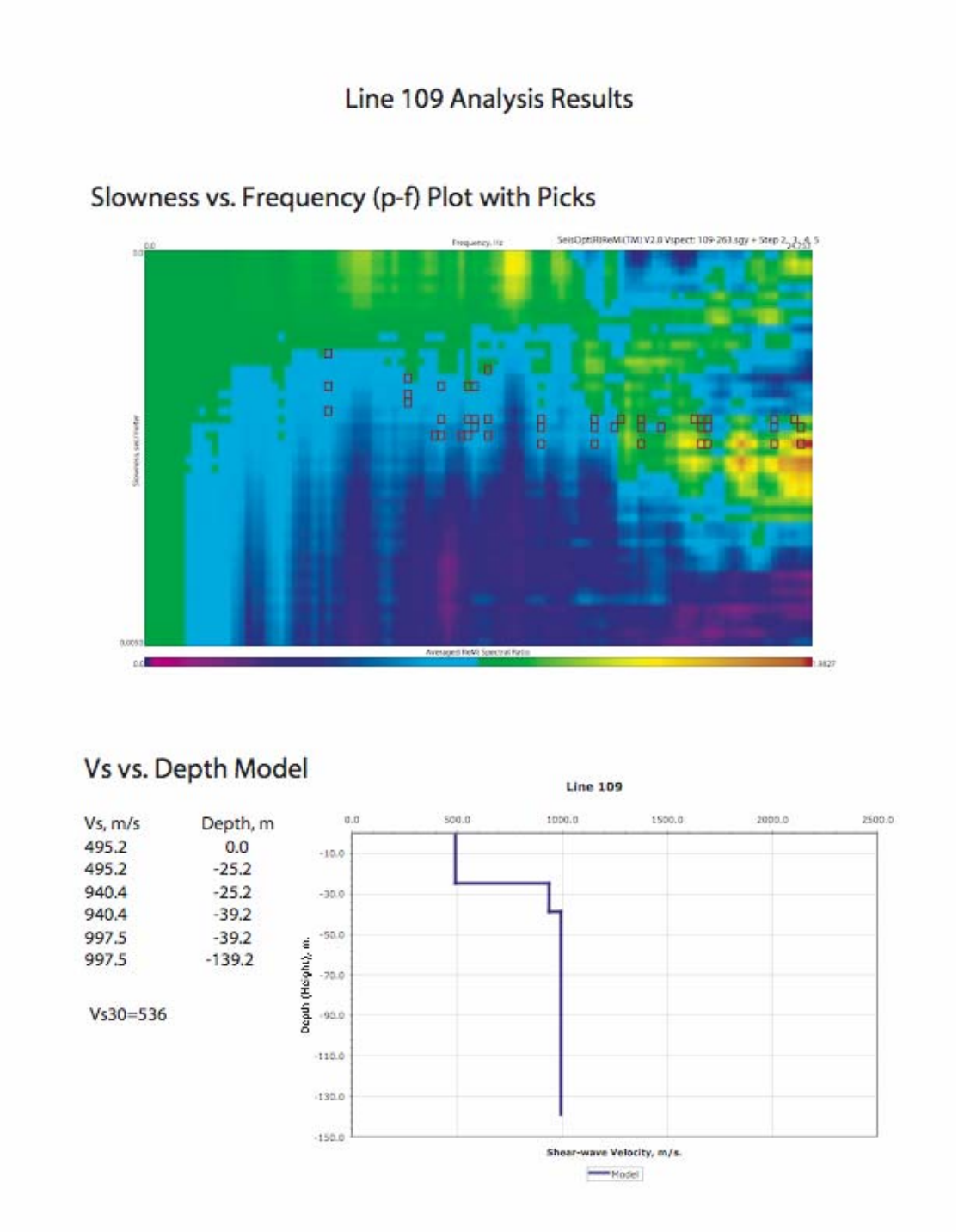

Figure 3. Analysis results for Line 109

Appendix 2: LABORATORY ESTIMATES OF TENSILE STRENGTHS FOR SAN ANDREAS SANDSTONES

Rock strength

Rock samples for strength testing were collected at outcrops. The rock was delivered to the rock mechanics lab as roughly shaped blocks, typically of the order of 1ft x 1 ft x 1ft, or somewhat larger. Most of the rock was too weak to be cored: the cement holding the grains together washed out during most attempts at coring. As a result very little core was obtained, barely sufficient for a few indirect tensile ("Brazilian") strength tests on disks and a few point load tests on core, and then only on the stronger rock types. Most strength testing was performed using lump point load testing, on irregularly shaped samples with dimensions typically of centimeters (inches). A few tensile strength tests were performed on "beams", roughly hand shaped short deep "beams" with approximately beam shapes. We performed three uniaxial compression tests on roughly handshaped prismoidal rock blocks. All testing was done under laboratory dry conditions.

Twelve indirect tensile splitting tests on Punchbowl sandstone give results ranging from 12.8 bar to 16.4 bar, with an average of 14.3 bar. Twelve lump point load tests on Punchbowl sandstone gave results ranging from 12.5 bar to 15.8 bar, with an average of 14.3 bar, a standard deviation of 1.47 bar. A second group of 42 tests on Punchbowl sandstone samples (prepared from different blocks) gives a mean tensile point load strength index of 1.5 bar, with a standard deviation of 1.245 bar, and a range from 0.08 bar to 4.2 bar. A third group of nine Punchbowl ss samples gives a point load strength index of 1.2 bar, with a standard deviation of 0.8 bar. A fourth group of five tests gives a point load strength index of 2.3 bar, standard deviation of 0.7 bar.

Ten lump point load tests on Cajon sandstone give point load strengths ranging from 0.4 bar to 2.8 bar, with an average value of 1.55 bar. The "beam" bending tests on Cajon sandstone, analyzed using simple beam formulas (i.e. not accounting for the geometry: short and deep), gave tensile strengths of 0.65 bar, 0.96 bar, and 1.56 bar, for an average of 1.1 bar, and surprisingly consistent given the rough shapes and obvious heterogeneity of the "rock", but the very low strength seems rather consistent with the obviously very low strength of the crumbly rock, grains of which frequently break out during simple handling.

The uniaxial compressive strengths of two samples of Cajon sandstone were 350 bar and 294 bar, with a tangent Young's modulus of about 20.7 kbar and 29.3 kbar respectively.

The uniaxial compressive strength of one Leona Valley sandstone sample was 352 bar, with an approximate tangent Young's modulus of 37.3 kbar.

Tests on "138 and 5 near Quail Lake" samples:

- diametrical splitting point load tensile strengths on core: 3 tests: 18.8 bar, 15.5 bar, 25.4 bar, for an average of 19.9 bar
- indirect tensile strength on discs (Brazilian), 5 samples from the same core: 15.9 bar to 25 bar, average 21.7 bar

- twenty two lump point load tests, average strength 3.25 bar, standard deviation 1.63 bar, range from 0.7 bar to 7.1 bar
- second group of lump point load tests (on samples from different block), six tests, average 1.75 bar, range from 0.18 to 3.55 bar

Lone Pine Canyon results: 52 point load tests on lumps, average 3.46 bar, standard deviation 1.25 bar.

Twelve lump point load tests have been performed on "conglomerate", giving a mean point load tensile strength index of 3.2 bar, with a standard deviation of 2.3 bar, and a range from 1.0 bar to 9.3 bar. The 9.3 bar value seems highly anomalous. When omitting it, the average value reduces to 2.66 bar, probably more representative for this group.

A few more results, from various locations:

- Red Rock Canyon: two results, lump point load tests, strength indices of 1.9 and 1.2 bar
- Cone Rock: one lump point load test: 3.0 bar
- Steep Cliff : four lump point load tests: average 1.65 bar, range 0.36 bar to 2.64 bar.

Indirect tensile strength testing was done according to ASTM D 3967-05, lump point load testing according to ASTM D 5731-05.

Some comments

The rock tested is extremely weak and variable. This creates a variety of testing problems, notably difficulties for sample preparation, and measuring forces at the lower range of our instrumentation capability (especially for strengths at or near 1 bar or less).

For several test series not enough tests were run to establish statistical validity.

Notwithstanding these limitations and qualifications, it is reasonable to conclude that the tensile strength of the weaker tested rocks probably is of the order of 4 bar or less, and the tensile strength of the stronger rocks tested is of the order of 15 to 20 bar. The higher strength values, obtained form splitting tensile strength tests on core, are biased: only the stronger rock can be cored.

The overwhelming majority of the results were obtained from point load tests on lumps, i.e. irregularly shaped samples with dimensions of the order of several to multiple cm. it was clear during testing that for many of these tests the loading points penetrate rather deeply into the specimens before splitting occurs. The depth of penetration is quite variable, presumably depending on the grain bounding strength in the contact areas, and probably ranges from less than 1 mm to more than 5 mm, possibly up to 10 mm. If one were to correct for the depth of penetration, and calculate the splitting tensile strength based on the distance between the loading

points at the time of splitting, the above listed point load strengths would increase by magnitudes ranging from negligible up to possibly 25%.

The results from the beam tests (internally surprisingly consistent) appear noticeably inconsistent with what we would usually expect for tensile testing. We would expect the beam strength to be of the order of twice the point load strength (e.g. Hudson and Harrison, 1997, p. 104; Jaeger and Cook, 1976, p. 191; Goodman, 1989, p. 66). Instead, the beam strengths measured here are only about two thirds of the point load strengths.

Even more surprising is the extraordinarily large ratio between the uniaxial compressive strength and the tensile strength of the Cajon sandstone, of the order of 200. The, literally, standard ratio ranges from 17.5 to 24.5 (depending on the sample size). (ASTM D 5731). The International Society for Rock Mechanics, in its recommended test procedure (ISRM, 1985), states that "On average, uniaxial compressive strength is 20-25 times point load strength … However, in tests on may different rock types the ratio can vary between 15 and 50 …" Johnston (1993), in a major review chapter on soft rock testing, states that a ratio of 22 is reasonable for rocks with a uniaxial compressive strength of 50-150 MPa, (500 to 1,500 bar). However, he references a major detailed investigation of this topic (Johnston, 1985), and concludes that for softer rocks the ratio decreases significantly, to about 10 to 7… Abdullah et al (2000), based on an investigation on twelve rock suites, admittedly mostly rather strong rocks, concluded that "*k* [ratio between compressive and tensile strength] can be even outside the range of 15 to 50 given in literature". Palchik and Hatzor (2004), based on an investigation that may be more relevant for the problem addressed here, concluded that for the weak chalks they tested, the ratio between uniaxial compressive strength and tensile strength is strongly porosity dependent, ranges from 8 – 18, and that "The difference between the observed ratio (8-18) and standard practice ($\sigma_c / I_d = 20\text{-}25$), according to ISRM suggested method (ISRM, 1985) can be as high as 127%." Brady and Brown (2004. p. 99), in their discussion of point load testing, state that "Very soft rocks, … are likely to give spurious results. A high degree of scatter is a general feature of point load test results and large numbers of individual determinations (often in excess of 100) are required in order to obtain reliable indices." Hoek and Bray, 1977, p. 96: " … , or if the points sink into the rock surface causing excessive crushing or deformation, the test should be rejected." These authors cite the same range of size dependent ratios of compressive to point load index tensile strength as later adopted by ASTM (ASTM D 5731). Unfortunately, they do not specify nor indicate what they consider "excessive crushing or deformation." Bowden et al (1998) argue that " … platen penetration may have an effect on the test results but it is an inherent factor in Pont Load testing on weaker rocks and does not invalidate the use of the Point Load test in any way, providing the effect is consistent." Admittedly, for the tests on which this conclusion is based, "The platen indention … was not more than 2 mm even for the softest chalk tested…"

Published results for weak rock generally find that the ratio of compressive strength to point load index tensile strength is lower, usually significantly lower, than the standard 17.5 to 24.5 range, Abbs, 1985, obtained a ratio of approximately 4, (3.7, ranging from 2.7 to 8.8), based on a total of nearly 800 tests on weak porous carbonate rocks, and concludes that " … the point load test is not very well suited to these materials …". Abbs quotes Haganaar (1983) who obtained a ratio of 3.2 for similar Arabian gulf materials, and a ratio of 3.8 to 4.9 for coral. Abbs (1985): " … the point load tests show a very wide scatter. This is probably because of crushing of the rock fabric

beneath the load points, which often occurs. In addition the results are affected by vugs in the rock specimen close to the points. Recently the larger investigations have included an on-board laboratory equipped to perform unconfined compression tests. This is considered a more appropriate solution because it appears that point load tests do not necessarily provide a reliable measurement of the strength of these rocks."

Bieniawski (1974, 1976), as quoted by Hoek and Brown (1980, p. 26), recommends that for rocks with a point load strength of less than 10 bar, or a uniaxial compressive strength of less than 250 bar, uniaxial strength testing be conducted, rather than point load testing.

References

Abbs, A.F., 1985, The use of the Point Load Index in Weak Carbonate Rocks, pp. 413-421, Strength Testing of Marine Sediments: Laboratory and In-Situ Measurements, ASTM STP 883, R.C. Chaney and K.R. Demars, Eds., American Society for Testing and Materials, Philadelphia.

Abdullah, Hasan, A.K. Dhawan, and A. Bandyopadhyay, 2000, Point load strength and uniaxial compressive strength, pp. 333-340, Site Characterisation Practice, Proceedings of the International Conference, Bangalore, India, December 6-8, 1999, Prakash C. Jha and R.N. Gupta, Eds., A.A. Balkema, Rotterdam/Brookfield.

ASTM D 3967-05, 2006, Standard Test Method for Splitting Tensile Strength of Intact Rock Core Specimens, Annual Book of ASTM Standards, Vol. 04.08, pp. 405 – 408, ASTM International, West Conshohocken, PA.

ASTM D 5731-05, 2006, Standard Test Method for Determination of the Point Load Strength Index of Rock, Annual Book of ASTM Standards, Vol. 04.09, pp. 82 – 89, ASTM International, West Conshohocken, PA.

Bieniawski, Z.T., 1974, Geomechanics classification of rock masses and its application in tunneling, Proc. Third International Congress on Rock Mechanics, ISRM, Denver, Vol. IIA, pp. 27-32, National Academy of Sciences, Washington, D.C.

Bieniawski, Z.T., 1976, Rock mass classification in rock engineering, Proc. Symposium on Exploration for Rock Engineering, Johannesburg, Vol. 1, pp. 97-106.

Bowden, A.J., J. Lamont-Black & S. Ullyott, 1998, Point load testing of weak rocks with particular reference to chalk, Quarterly Journal of Engineering Geology, Vol. 31, pp. 95-103.

Goodman, R.E., 1989, Introduction to Rock Mechanics, Second Edition, John Wiley & Sons, New York.

Haganaar, J., 1983, Discussion to Conference on Piling and Ground Treatment, Institution of Civil Engineers, London, March, p.111 (as referenced by Abbs, 1985).

Hoek, E., and J.W. Bray, 1977, Rock Slope Engineering, Revised Second Edition, The Institution of Mining and Metallurgy, London.

Hoek, E., and E.T. Brown, 1980, Underground Excavations in Rock, The Institution of Mining and Metallurgy, London.

Hudson, J.A., and J. P. Harrison, 1997, Engineering Rock Mechanics, Pergamon, Amsterdam.

ISRM, 1985, Suggested Method for Determining Point Load Strength, Int. Jnl. of Rock Mechanics Min. Sci. & Geomech. Abstr., Vol. 22, No. 2, pp. 51-60.

Jaeger, J.C. and N.G.W. Cook, 1976, Fundamentals of Rock Mechanics, Second Edition, Chapman and Hall, London, A Halsted Press Book, John Wiley & Sons, Inc., New York.

Johnston, I.W., 1985, Strength of Intact Geomechanical Materials, J. Geotech. Eng., Am. Soc. Civ. Eng., Vol. 111, pp. 730-749.

Johnston, I.W., 1993, Soft Rock Engineering, Ch. 15, pp. 367 – 393 of Comprehensive Rock Engineering, John A. Hudson, Editor-in-Chief, Vol. 1, Fundamentals, Edwin T. Brown, Volume Editor, Pergamon Press, Oxford.

Palchik, V. and Y.H. Hatzor, 2004, The Influence of Porosity on Tensile and Compressive Strength of Porous Chalks, pp. 331-341, Rock Mech. Rock Engng., Vol. 37, Issue 4.

Appendix 3: CALCULATION OF TENSILE STRESSES FOR SAN ANDREAS SANDSTONES

As outlined in the text, relic sandstones exist within ~ 5 km of the San Andreas fault between Tejon and Cajon passes in southern California. The sandstones exist on both sides of the fault and may have been exhumed from depths exceeding 1 km. The tensile strength measurements of surface samples, presented in Appendix 2, demonstrate that the sandstones are very weak in tension. We wish to address the following question: what ground motion amplitudes are required to fracture these sandstones? In this appendix a method is outlined to calculate the stresses induced near the surface of a uniform half-space by steady-state, sinusoidal plane S-waves. This work does not presume either the wave types or orientations which are emanating from the earthquake source. Instead induced stresses are calculated as a function of angle of incidence and depth for plane S-waves with varying frequency, amplitude, and wave type. Subsequent discussions follow the work presented in Chapter 5 of Aki and Richards (2002). P-wave results have been omitted as they do not contribute significantly to the ground motions in the near field.

Suppose that a wave propagates through an isotropic, elastic medium. Strain is given by

$$\varepsilon_{ij} = \frac{1}{2}\left(\frac{\partial u_i}{\partial x_j} + \frac{\partial u_j}{\partial x_i} \right) (A3.1)$$

where u_i is the displacement in the ith direction. Stress-strain relations for this material provide that

$$\sigma_{ij} = \lambda\left(\frac{\partial u_1}{\partial x_1} + \frac{\partial u_2}{\partial x_2} + \frac{\partial u_3}{\partial x_3} \right)\delta_{ij} + 2\mu\varepsilon_{ij} (A3.2)$$

where λ is the second of Lame's constants and μ is the shear modulus. In this case the stress tensor will be symmetric (e.g., $\sigma_{ij} = \sigma_{ji}$). In order to calculate the stresses induced by a propagating wave, one must have explicit knowledge of the displacement as a function of space. As mentioned above, steady-state wave propagation of plane S-waves of various types will be investigated in this analysis.

The displacements of upgoing and downgoing SH waves are given respectively by

$$USH = (0, S, 0)\exp\left[i\omega\left(\frac{\sin j}{\beta} x_1 - \frac{\cos j}{\beta} x_3 - t \right) \right] (A3.3.1)$$

$$DSH = (0, S, 0)\exp\left[i\omega\left(\frac{\sin j}{\beta} x_1 + \frac{\cos j}{\beta} x_3 - t \right) \right] (A3.3.2)$$

where j is the angle of incidence of the SH wave, β is the shear wave velocity, x_1 the horizontal coordinate, x_3 is the vertical coordinate, ω is the frequency, and t is time. $(0, S, 0)$ is the amplitude of the displacement wave in x_1, x_2, and x_3 coordinates, respectively. The strains and

stresses can be easily calculated from the definitions given in equations *A3.1* and *A3.2*. Notice for SH waves $\sigma_{11} = \sigma_{22} = \sigma_{33} = \sigma_{13} = 0$. The shear stresses $\sigma_{12} = \sigma_{21}, \sigma_{23} = \sigma_{32}$ are given by

$$\sigma_{12} = S\mu i\omega \frac{\sin j}{\beta}\left[USH + DSH\right] = 2S\mu i\omega \frac{\sin j}{\beta}\cos\left(\omega \frac{\cos j}{\beta} x_3\right)\exp\left[i\omega\left(\frac{\sin j}{\beta}x_1 - t\right)\right] \quad (A3.4.1)$$

$$\sigma_{23} = S\mu i\omega \frac{\cos j}{\beta}\left[DSH - USH\right] = -2S\mu\omega \frac{\cos j}{\beta}\sin\left(\omega \frac{\cos j}{\beta} x_3\right)\exp\left[i\omega\left(\frac{\sin j}{\beta}x_1 - t\right)\right] \quad (A3.4.2).$$

For the case of an SV wave impinging upon the free surface, the displacement of the upward propagating wave is of the form

$$USV = S(\cos j, 0, \sin j)\exp\left[i\omega\left(\frac{\sin j}{\beta}x_1 - \frac{\cos j}{\beta}x_3 - t\right)\right] \quad (A3.5).$$

Whereas the SH particle motion is in the x_2 direction, the SV particle motion is in both the x_1 and x_3 directions. As the SV wave encounters the free surface, the SV wave is reflected and P and Rayleigh waves can also be produced. The downgoing P and SV displacements are given by

$$DP = S(\sin i, 0, \cos i)\overset{/}{S}\overset{\backslash}{P}\exp\left[i\omega\left(\frac{\sin i}{\alpha}x_1 + \frac{\cos i}{\alpha}x_3 - t\right)\right] \quad (A3.6.1)$$

$$DSV = S(\cos j, 0, -\sin j)\overset{/}{S}\overset{\backslash}{S}\exp\left[i\omega\left(\frac{\sin j}{\beta}x_1 + \frac{\cos j}{\beta}x_3 - t\right)\right] \quad (A3.6.2)$$

where $i = \sin^{-1}\left(\frac{\alpha \sin j}{\beta}\right)$ is the angle at which the P wave propagates from the free surface and α is the P-wave velocity. The P conversion and SV reflection coefficients, $\overset{/}{S}\overset{\backslash}{P}$ and $\overset{/}{S}\overset{\backslash}{S}$ are given by

$$\overset{/}{S}\overset{\backslash}{P} = \frac{4\frac{\beta}{\alpha}p\frac{\cos j}{\beta}\left(\frac{1}{\beta^2} - 2p^2\right)}{\left(\frac{1}{\beta^2} - 2p^2\right)^2 + 4p^2\frac{\cos i}{\alpha}\frac{\cos j}{\beta}} \quad (A3.7.1)$$

$$\overset{/}{S}\overset{\backslash}{S} = \frac{\left(\frac{1}{\beta^2} - 2p^2\right)^2 - 4p^2\frac{\cos i}{\alpha}\frac{\cos j}{\beta}}{\left(\frac{1}{\beta^2} - 2p^2\right)^2 + 4p^2\frac{\cos i}{\alpha}\frac{\cos j}{\beta}} \quad (A3.7.2)$$

where $p = \frac{\sin i}{\alpha} = \frac{\sin j}{\beta}$ is the ray parameter. For $j <= \sin^{-1}\left(\frac{\beta}{\alpha}\right)$, the above relations produce real valued conversion and reflection coefficients. For $\frac{\pi}{2} > j > \sin^{-1}\left(\frac{\beta}{\alpha}\right)$, evanescent Rayleigh waves will be produced. In this work it is assumed that the Poisson ratio $\nu = 0.25$ so that

$\alpha = \sqrt{3}\beta$. In other words, for angles of incidence greater than ~ 35.3° from vertical, evanescent waves will be produced. For $\frac{\pi}{2} > j > \sin^{-1}\left(\frac{\beta}{\alpha}\right)$,

$$\frac{\cos i}{\alpha} = \pm i\sqrt{p^2 - \frac{1}{\alpha^2}} \quad (A3.8)$$

for $\omega > 0$ and $\omega < 0$, respectively. This ensures that the P-wave amplitude does not exponentially increase with depth. The conversion and reflection coefficients outlined above take on imaginary values in this situation. In this case the stress tensor will also be symmetric and $\sigma_{12} = \sigma_{23} = 0$.

A number of criteria have been used in rock mechanics and engineering practice to determine whether or not stresses of a specified level produce yielding in solids. As the tensile strength of a material is generally much lower than the compressive (perhaps by a factor of 10-20 as discussed in Appendix 2) or shear strengths, these analyses first require transformation of the stress tensor into the principle stress directions. In other words, a set of rotations about the system of axes are sought which produce only tensile and compressive stresses. The diagonalization of the stress tensor is achieved by calculating the eigenvalues and eigenvectors of the stress tensor; the eigenvalues are the principle stresses ($\sigma_3 \geq \sigma_2 \geq \sigma_1$) and the eigenvectors provide the angles of rotation about the orthogonal axes which are required to produce the principle stress state. Note that as plane waves are oscillatory in nature, both the amplitudes and directions of the principle stresses will oscillate as a function of time from compressive ($\sigma_i < 0$) to tensile ($\sigma_i > 0$) at a particular point in space.

This work utilizes the Mohr-Coulomb failure criteria. Suppose that σ_c and σ_t are the compressive and tensile strengths, respectively. The Mohr-Coulomb yield criteria may be expressed as:

$$\pm\frac{\sigma_1 - \sigma_2}{2} = c - K\left(\frac{\sigma_1 + \sigma_2}{2}\right); \pm\frac{\sigma_2 - \sigma_3}{2} = c - K\left(\frac{\sigma_2 + \sigma_3}{2}\right); \pm\frac{\sigma_3 - \sigma_1}{2} = c - K\left(\frac{\sigma_3 + \sigma_1}{2}\right) \quad (A3.9)$$

where

$$m = \frac{\sigma_c}{\sigma_t}, K = \frac{m-1}{m+1}, c = \left(\frac{1}{m+1}\right)\sigma_c \quad (A3.10).$$

A lithostatic stress state is assumed throughout the subsequent analysis which requires that the overburden stress be subtracted from each of the normal stresses, $\sigma_{11}, \sigma_{22}, \sigma_{33}$, prior to calculation of the principle stresses. Principle stresses are calculated for each angle of incidence, depth, and instance of time. For $\sigma_1 > 0$ (e.g., tensile maximum principle stress), the calculated principle stresses are compared with the Mohr-Coulomb failure criteria. In the following analysis σ_c = 350 bars and σ_t = 20 bars which are consistent with some of the strongest sandstone samples reported in Appendix 2.

Figures A3.1, A3.2, and A3.3 present the ground velocities which exceed the Mohr-Coulomb failure criteria for plane SH waves. The shear wave velocity has been assigned the value 2000 m/s and the density is 1.9 gm/cm^3 in all subsequent calculations. The three figures correspond to

plane waves with frequencies 0.5 Hz, 1 Hz, and 2 Hz, respectively. As the majority of seismic energy may be released from depth on the fault, the velocity constraints are derived for angles of incidence less than 30 degrees. As these figures demonstrate, yielding occurs at depths approaching one-quarter of the specified wavelength (e.g., 1000 m, 500 m, and 250 m for 0.5 Hz, 1 Hz, and 2 Hz waves, respectively). The addition of lithostatic stress produces yielding at shallower depths than one-quarter wavelength. These calculations suggest that plane SH waves with frequencies 0.5 Hz, 1 Hz, and 2 Hz would produce yielding should their peak velocities be greater than approximately 200 cm/s, 120 cm/s, and 80 cm/s, respectively. SH waves with large angles of incidence (> 60 degrees) produce significant yielding very near the free surface (within ~ 20 m) when the particle velocities are as low as 30 cm/s. Significant SH energy may not be produced in the near field of large earthquakes, though.

The stress model used to derive the results above corresponds to the situation with no tectonic stress ($\sigma_{12} = \sigma_{21} = 0$). Figures A3.4, A3.5, and A3.6 investigate a high tectonic stress model where $\bar{\sigma}_{12} = \sigma_{12} + 0.65\rho g z$ (ρ is the density, g is the acceleration of gravity, and z is the depth). This tectonic stress state is consistent with frictional values obtained from rock mechanics experiments. As these figures demonstrate, yielding occurs at somewhat lower peak particle velocities for SH waves with shallow angles of incidence (160 cm/s, 100 cm/s, and 70 cm/s for 0.5 Hz, 1 Hz, and 2 Hz plane SH waves, respectively). A low tectonic stress model, say $\bar{\sigma}_{12} = \sigma_{12} + 0.2\rho g z$, would be similar to the results presented in figures A3.1, A3.2, and A3.3.

Figures A3.7, A3.8, and A3.9 show results for the lithostatic stress case without tectonic stress where the shear wave velocity is 1000 m/s. Yielding occurs for shallow angles of incidence at about 240 cm/s, 160 cm/s, 110 cm/s for 0.5 Hz, 1 Hz, and 2 Hz plane SH waves, respectively. Additionally the one-quarter wavelength depth has been diminished to 500 m, 250 m, and 125 m for the three cases, leading to yielding very near to the free surface.

Figures A3.10, A3.11, and A3.12 depict contours of ground velocity which exceed the Mohr-Coulomb failure criteria for plane SV waves with shear wave velocity 2000 m/s. These figures also correspond to plane waves with frequencies 0.5 Hz, 1 Hz, and 2 Hz, respectively. As with the SH case outlined above, the minimum velocities producing significant yielding occur near one-quarter wavelength depths. These velocities are approximately 200 cm/s, 120 cm/s, and 80 cm/s for the 0.5 Hz, 1 Hz, and 2 Hz cases, respectively, for SV waves at shallow incidence. Near the transition where Rayleigh waves are produced (35.3 degrees), very high stresses are induced which would produce yielding with very low velocities down to significant depths. This is in contrast to the SH behavior demonstrated in Figures A3.1, A3.2, and A3.3. These results correspond to the situation with no tectonic stress ($\sigma_{12} = \sigma_{21} = 0$). Figures A3.13, A3.14, and A3.15 assume a high tectonic stress model (e.g., $\sigma_{12} = \sigma_{21} = 0.65\rho g z$). This reduces the velocities leading to failure to approximately 160 cm/s, 100 cm/s, and 70 cm/s for the 0.5 Hz, 1 Hz, and 2 Hz cases, respectively. These results are very similar to the SH case outlined above for plane waves with shallow angles on incidence.

As the Subtask 1 report by John Anderson outlines, there have been 13 recordings of earthquakes in continental strike-slip environments where the peak 3D particle velocities exceed 100 cm/s. Should S-wave ground motions of this amplitude occur at the sandstone sites with predominant

frequencies greater than 1 Hz, the sandstones would yield at depths less than 500 meters. While the current outcrops were buried at this depth, yielding did not occur as evidenced by the lack of fracturing at any scale. Though the time period that the current outcrop was at depth is speculative, there is no doubt that it has passed through that depth range at some point in the past.

References

Aki, K. and P.G. Richards (2003). Quantitative Seismology, 2nd Edition. Sausalito, Ca : University Sceince Books.